

RESEARCH ARTICLE

 **Bora Tetik**¹
 **Hasan Ucuzal**²
 **Seyma Yasar**²
 **Cemil Colak**²

¹Department of
Neurosurgery, Faculty of
Medicine, Inonu
University, Malatya,
Turkey

²Department of Biostatistics
and Medical Informatics
Faculty of Medicine, Inonu
University, Malatya,
Turkey

Corresponding Author:
Seyma Yasar

Department of Biostatistics
and Medical Informatics
Faculty of Medicine, Inonu
University, Malatya, Turkey
Phone: +90 507 639 7121
mail:seyma.yasar@inonu.edu.tr

Received: 02.03.2021
Acceptance: 04.05.2021
DOI: 10.18521/ktd.889777

Konuralp Medical Journal
e-ISSN1309-3878
konuralptipdergi@duzce.edu.tr
konuralptipdergisi@gmail.com
www.konuralptipdergi.duzce.edu.tr

Automated Classification of Brain Tumors by Deep Learning-Based Models on Magnetic Resonance Images Using a Developed Web-Based Interface

ABSTRACT

Objective: Primary central nervous system tumors (PCNSTs) compose nearly 3% of newly diagnosed cancers worldwide and are more common in men. The incidence of brain tumors and PCNSTs-related deaths are gradually increasing all over the world. Recently, many studies have focused on automated machine learning (AutoML) algorithms which are developed using deep learning algorithms on medical imaging applications. The main purposes of this study are -to demonstrate the use of artificial intelligence-based techniques to predict medical images of different brain tumors (glioma, meningioma, pituitary adenoma) to provide technical support to radiologists and -to develop a user-friendly and free web-based software to classify brain tumors for making quick and accurate clinical decisions.

Methods: Open-sourced T1-weighted magnetic resonance brain tumor images were achieved from Nanfang Hospital, Guangzhou, China, and General Hospital, Tianjin Medical University. To construct the proposed system which web-based interface and the deep learning-based models, the Keras/Auto-Keras library, which is employed in Python's programming language, is used. Accuracy, sensitivity, specificity, G-mean, F-score, and Matthews correlation coefficient metrics were used for performance evaluations.

Results: While 80% (2599 instances) of the dataset was used in the training phase, 20% (465 instances) was employed in the testing phase. All the performance metrics were higher than 98% for the classification of brain tumors on the training data set. Similarly, all the evaluation metrics were higher than 91% except for sensitivity and MCC for meningioma on the testing dataset.

Conclusions: The results from the experiment reveal that the proposed software can be used to detect and diagnose three types of brain tumors. This developed web-based software can be accessed freely in both English and Turkish at <http://biostatapps.inonu.edu.tr/BTSY/>.

Keywords: Brain Tumors, Deep-Learning Strategy, Keras/Auto-Keras, T1-Weighted Magnetic Resonance Imaging.

Geliştirilmiş Bir Web Tabanlı Arayüz Kullanarak Beyin Tümörlerinin Manyetik Rezonans Görüntülerinde Derin Öğrenme Tabanlı Modellerle Otomatik Sınıflandırılması

ÖZET

Amaç: Primer santral sinir sistemi tümörleri (PSSST), dünyada yeni teşhis edilen kanserlerin yaklaşık %3'ünü oluşturmaktadır ve erkeklerde sıklığı daha yüksektir. Beyin tümörlerinin ve PSSST'lere bağlı ölümlerin görülme sıklığı tüm dünyada giderek artmaktadır. Son zamanlarda birçok çalışma, tıbbi görüntüleme uygulamalarında derin öğrenme algoritmaları kullanılarak geliştirilen otomatik makine öğrenimi (AutoML) algoritmalarına odaklanmıştır. Bu çalışmanın temel amacı, radyologlara destek sağlamak için beyin tümörlerinin (glioma, menenjiom hipofiz adenomları) tıbbi görüntülerinin analizinde yapay zeka tabanlı tekniklerin kullanımını göstermek, hızlı ve doğru tanı konulması için beyin tümörlerini sınıflandıran kullanıcı dostu ve 'ücretsiz web tabanlı bir yazılım geliştirmektir.

Gereç ve Yöntem: Açık kaynaklı T1 ağırlıklı manyetik rezonans beyin tümörü görüntüleri Nanfang Hastanesi, Guangzhou, Çin ve Genel Hastane, Tianjin Tıp Üniversitesinden elde edildi. Önerilen web tabanlı arayüzün ve derin öğrenme tabanlı modellerin oluşturulması için Python'un programlama dilinde kullanılan Keras / Auto-Keras kütüphanesi kullanıldı. Performans değerlendirmelerinde doğruluk, duyarlılık, özgüllük, G-ortalama, F-skor ve Matthews korelasyon katsayısı ölçümleri kullanıldı.

Bulgular: Eğitim aşamasında veri kümesinin %80'i (2599 örnek) kullanılırken, %20'si (465 örnek) test aşamasında kullanıldı. Eğitim veri setinde beyin tümörlerinin sınıflandırılmasında tüm performans ölçütleri %98'in üzerinde sonuçlanmıştır. Benzer şekilde, test veri setinde menenjiom için duyarlılık ve MCC dışındaki tüm değerlendirme ölçütleri % 91'den yüksektir.

Sonuç: Deneysel sonuçlar, önerilen yazılımın üç tip beyin tümörünü tespit etmek ve tanı koymak için kullanılabileceğini ortaya koymaktadır. Geliştirilen bu web tabanlı yazılıma hem İngilizce hem de Türkçe olarak <http://biostatapps.inonu.edu.tr/BTSY/> adresinden ücretsiz olarak erişilebilir.

Anahtar Kelimeler: Beyin Tümörleri, Derin Öğrenme Yaklaşımları, Keras / Auto-Keras, T1 Ağırlıklı Manyetik Rezonans Görüntüleme

INTRODUCTION

Primary central nervous system tumors (PCNSTs) are a group of heterogeneous diseases containing more than 100 histological types which are classified according to their morphological and etiological properties, clinical behavior, localization, and molecular structures at the 2016 World Health Organization (WHO) Classification of Tumors of the Central Nervous System (1, 2). PCNSTs are consisting nearly 3% of newly diagnosed cancers worldwide and are more common in men than in women (3). Technological effect due to the increase in the use of assistive tools in diagnosing MRI, the incidence of brain tumors and PCNSTs-related deaths are gradually increasing all over the world. The incidence of PCNSTs ranges from 17.6 / 100000 to 22.0/100000 in Europe and the United States, respectively (4, 5). The incidence of glial tumors in Turkey is 3.3/100000. Although the average 5-year survival for PCNSTs is 33.4%, this period varies according to specific tumor subgroups; such as 100% for pilocytic astrocytoma, 58% for low-grade astrocytoma, 11% for anaplastic astrocytoma, and 1.2% for glioblastoma (6, 7).

The central nervous system tumors can be classified as benign and malignant according to their behaviour. According to WHO, Grade I and II tumors are considered as low grade and benign, while grade III and IV tumors are evaluated as high grade or malignant (1). Approximately two-thirds of central nervous system tumors are benign. Almost 80% of malignant primary central nervous system tumors are gliomas, which make up about one-third of brain tumors. More than half of the diagnosed gliomas are glioblastoma or WHO grade IV tumors (8). Although the incidence of glial tumors exhibits regional changes, the global incidence of all glial tumors is generally 2.98/100000 (9). Although computed tomography is used as the first imaging method in the identification of central nervous system tumors, conventional MR imaging is the basis for the imaging of the central nervous system gliomas in general, while low-grade gliomas emerge hypointense on T1-weighted imaging, hyperintense, and minimal mass effect on T2-weighted imaging. As the tumor stage progresses, irregular borders with poorly defined mass effect and peripheral edema effect become more heterogeneous (10).

Meningiomas, which form more than a third of all primary central nervous system tumors, are the most common primary intracranial tumors in adults. Its annual incidence is 8.3/100000, and it is more common in women than in men (11). Meningiomas are tumors arising from the arachnoid valve cells (1). According to WHO 2016 classification, meningiomas are examined in three grades as grade I (benign meningioma) 81%, grade II (atypical meningioma) 17%, grade III (malignant meningioma) 2% (11). Computed tomography can

be used to identify the lesion and for initial imaging. MR imaging is the most commonly used method for the diagnosis of additional lesions and tumor contours with higher resolution images of intracranial soft tissue. Classically, meningiomas are seen in T1 weighted images and T2 weighted images hyperintense compared to parenchyma, and significant peripheral edema area can be observed in subtypes such as secretory meningiomas (12). The second most common intracranial masses after meningiomas are pituitary adenomas (pituitary tumor) (13). It is a heterogeneous group of lesions that are generally benign in the central nervous system (14). The estimated prevalence in the general population is 16.7% (13). Pituitary adenomas can develop a broad clinical presentation. Many pituitary adenomas do not show symptoms, and while detected incidental, some pituitary adenomas may demonstrate slow-developing nonspecific symptoms and thus may cause delays in the diagnosis and treatment (14). Functional pituitary adenomas can occur with specific symptoms such as hormonal disorders, pressure on the optic nerve, visual field disorders, and organomegaly, with Cushing syndrome, acromegaly/gigantism, hyperthyroidism, or hypogonadism due to hyperprolactinemia (15). MR imaging is used to identify lesions in the pituitary gland and the parasellar region. The standard anterior pituitary gland appears in T1 and T2-weighted images as isointense against gray matter, while the posterior pituitary gland appears in T1-weighted imaging rather than hyperintense and T2-weighted imaging (13, 14). If the patient has symptoms and signs suggesting a brain tumor, radiological imaging should be performed to prove or rule out the presence of the lesion. In a patient with suspected primary central nervous system tumor, the most important imaging method that can provide the necessary information in diagnosis, treatment, and follow-up is MR imaging.

Artificial Intelligence (AI) methods show promise to assist in detecting and assessing image-based tasks, depending on the curing of high-quality training sets. AI technology today provides numerous invaluable tools for intelligent data analysis to solve various medical problems, particularly diagnostic tasks. AI, with its powerful capabilities, seems to be a possible candidate for that role. On the other hand, AI applications ultimately need the radiomics in medical image analysis because the metrics used to train and develop the AI models are provided via radiomics approaches, specifically feature extraction/engineering methods. Examining, interpreting, and reporting MR images can lead to loss of time and/or rarely misinterpretation during the diagnosis phase of the patient. Computer-aided automatic detection and diagnosis systems based on deep learning and image processing algorithms

have been used recently to minimize both the interpretation time of the MR images and the margin of error in the interpretation (16, 17). Deep learning is an artificial intelligence method that uses multi-layered neural networks in object recognition and image classification and is one of the types of machine learning. Instead of learning with encoded rules that differ from the classic machine learning methods, deep learning can automatically learn from the icons of data such as pictures, videos, audio, text, etc. (6).

The main purpose of this study is to demonstrate the use of artificial intelligence-based techniques to predict medical images of different brain tumors to provide clinical support to radiologists. The secondary aim is to develop a user-friendly, free web-based software that can classify brain tumors (glioma, meningioma, pituitary adenomas) and enable specialists to make quick and accurate clinical decisions.

MATERIAL AND METHODS

Dataset: The proposed technique in this study depends on 2D slices. Since typically just a specific number of brain contrast-enhanced MRI with a considerable slice gap are achieved and accessible, the improvement of a 2D picture-based classification for medical applications may be increasingly functional. In the present study, the open-sourced brain tumor images were achieved from Nanfang Hospital, Guangzhou, China, and General Hospital, Tianjin Medical University, China (18). The dataset contained 3064 T1-weighted contrast-enhanced magnetic resonance (MR) images from 233 patients, which included 708 meningiomas, 1426 gliomas, and 930 pituitary tumors. The brain tumor images have an in-plane resolution of 512×512 with a pixel size of $0.49 \times 0.49 \text{ mm}^2$. The thickness and gap of the slice are 6 mm and 1 mm, respectively. The tumor boundary was manually outlined by experienced radiologists (19, 20).

The Proposed Auto-Keras System Based on Deep Learning: Machine learning is a system making forward predictions with a computational model created through sample data and experiences, or making statistical inferences about the structure and distribution of existing data (21). Deep learning, a machine learning sub-branch, is an algorithm that tries to model high-level abstractions of data. In other words, deep learning is an area that develops in the field of machine learning, with very

Image preprocessing techniques can improve the classification performance of MR images. In the current study, image rotation, changing width and length, truncating images, rescaling, noise removal approaches, inhomogeneity correction, etc. procedures were applied to the studied MR images for image pre-processing. The dataset used in the development of the deep learning model consists of 3064 T1-weighted MR images of glioma, meningioma, pituitary tumors. To examine the

complex layers for processing information nonlinearly. This technique takes its deep name from its deep layers and hierarchical structure (22). Many deep learning techniques have a deeper structure than artificial neural networks. Convolutional Neural Network (CNN), one of these techniques, works forward-looking like artificial neural networks. However, this technique has a feature extraction layer that is not found in artificial neural networks. The main components of CNN are convolution layer, pooling layer, activation functions, fully connected layer, loss layer, regularization, and optimization (23).

Automated machine learning (AutoML) is a fully automated process that starts with the preprocessing of the machine learning (ML) algorithms and ends with the model processing to achieve the best results on a data set (24). It is aimed to minimize human errors in the classical machine learning process with AutoML, which has been used frequently recently. One of the fundamental problems of ML is hyperparameter optimization. While this process in the ML is carried out depending on the experience of the individual, it is performed automatically in the AutoML (25, 26).

Auto-Keras, an AutoML tool, is an open-source Python library created using the Keras deep learning architecture(s). Using the Bayesian optimization method, one of the AutoML approaches, Auto-Keras creates multiple models with a different number of layers and determines the model with the best performance among these models (27). The detailed description of the Auto-Keras system is given in Figure 1.

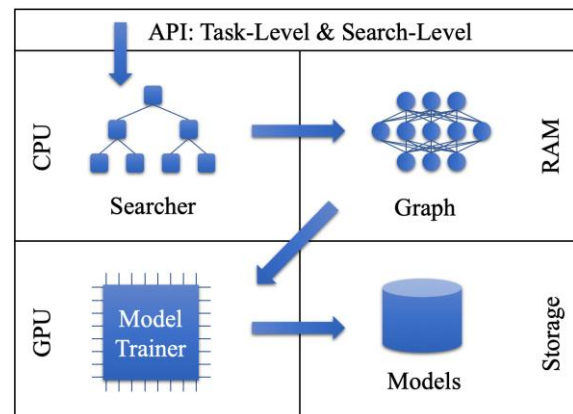


Figure 1. The detailed description of Auto-Keras system (27)

validity and performance of the deep learning model, while 80% (2599 instances) of the whole dataset is used in the training phase, 20% (465 instances) of the whole dataset are employed in the testing phase. H5py (28), random, Matplotlib, NumPy, and OpenCV libraries for Python programming language are used in the image preprocessing operations described earlier.

Development of The Web-Based Software resting On the Proposed Model: The developed

web-based software can classify glioma, meningioma, and pituitary tumors over T1-weighted MR images. The open-sourced web software developed by using TensorFlow, Keras, Scikit-learn, OpenCV, Pandas, NumPy,

Matplotlib, and Flask libraries of Python programming language is available in Turkish and English at <http://biostatapps.inonu.edu.tr/BTSY/>. The screenshot of the developed web-based software is given in Figure 2.

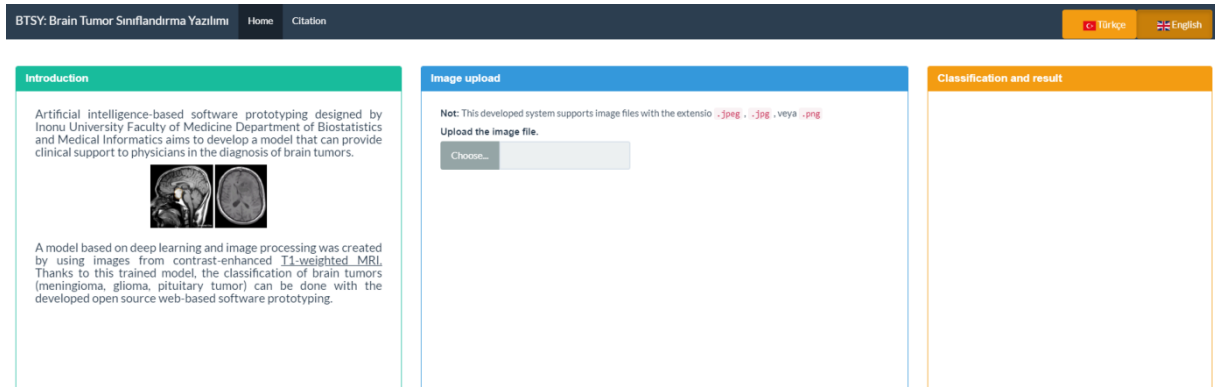


Figure 2. Screenshot of the English web page

The "Home" menu, the first main menu of the developed web-based software, consists of 3 sub-sections: "Introduction", "Image Upload", and "Classification and Result". The "Introduction" sub-section contains information about the operating principle of the software. The T1-weighted MR image of the brain tumor to be analyzed is loaded in the "Image Upload" sub-section. Finally, the type of brain tumor loaded into the system is estimated in the "Classification and Result" sub-section. Since the developed software supports image files with ".jpeg", ".jpg" and ".png" extensions, if a file extension other than these three file extensions is uploaded to the system, the warning in Figure 3 will be displayed in the "Classification and Result" sub-section.

For the filter created to identify the images of irrelevance loaded into the software, at the first stage, all components of the "mxn" pixel matrix calculated for each image are summed with the help of the following formula, and the min-max range is determined for these values.

$$A_F = \sum_{i=1}^m \sum_{j=1}^n a_{ij}$$

Then, images other than these values are defined as irrelevant images. The pseudo-code for this filter is as follows.

PSEUDO-CODE I. MIN-MAX FILTERING

A, B, and C are matrices of each RGB channel of uploaded images.

```

1: if (A, B and C are not all equal){
2:   return ("Irrelevant image")
3: } else {
4:   if (AF not in range [192249, 293860]) {
5:     return ("Irrelevant image")
6:   }
7:   else {
8:     return ("Relevant image")
9:   }
10: }

```

Performance evaluation

Performance assessment of the proposed model(s) is performed using evaluation metrics like accuracy, sensitivity, specificity, G-mean, F-score, and Matthews correlation coefficient (MCC). Abbreviations used in these formulas represent TP: true positive number, TN: true negative number, FP: false positive number, and FN: false negative number, respectively (29).

$$\text{Accuracy} = (\text{TP} + \text{TN}) / (\text{TP} + \text{TN} + \text{FP} + \text{FN})$$

$$\text{Sensitivity} = \text{TP} / (\text{FN} + \text{TP})$$

$$\text{Specificity} = \text{TN} / (\text{FP} + \text{TN})$$

$$\text{G-mean} = (\text{Sensitivity} * \text{Specificity})^{1/2}$$

$$\text{F-score} = 2\text{TP} / (2\text{TP} + \text{FP} + \text{FN})$$

$$\text{MCC} = (\text{TP} * \text{TN} - \text{FP} * \text{FN}) / ((\text{TP} + \text{FP}) * (\text{TP} + \text{FN}) * (\text{TN} + \text{FP}) * (\text{TN} + \text{FN}))^{1/2}$$



Figure 3. Unsupported file extension type error

RESULTS

The performance metrics on the training and testing datasets of the developed deep learning model and the 95% confidence intervals for these metrics are given in Table 1.

When the performance metrics are taken into account, the performance of the developed model to

classify brain tumors (Glioma/Meningioma/Pituitary adenomas) is quite successful in both the training dataset and the testing dataset. The detailed summary information of the proposed Auto-Keras model based on deep learning is given in Table 2.

Table 1. The performance metrics and 95% confidence intervals for the training and testing datasets

Metrics	Training Value (%) (95% CI)			Testing Value (%) (95% CI)		
	Meningioma	Glioma	Pituitary adenomas	Meningioma	Glioma	Pituitary adenomas
Accuracy	99.81 (99.64-99.98)	99.77 (99.58-99.95)	99.65 (99.43-99.88)	96.29 (94.57-98.01)	96.08 (94.31-97.84)	97.14 (95.62-98.65)
Precision	99.84 (99.68-99.99)	99.92 (99.81-99.99)	98.98 (98.60-99.37)	94.51 (92.43-96.58)	96.97 (95.41-98.53)	91.61 (89.09-94.13)
Sensitivity	99.35 (99.05-99.66)	99.58 (99.34-99.83)	99.87 (99.73-99.99)	87.76 (84.78-90.73)	95.32 (93.40-97.24)	99.24 (98.45-99.99)
Specificity	99.95 (99.86-99.99)	99.93 (99.83-99.99)	99.56 (99.31-99.81)	98.61 (97.55-99.67)	96.88 (95.29-98.46)	96.27 (94.55-97.99)
F-Score	99.60 (99.35-99.84)	99.75 (99.56-99.94)	99.43 (99.14-99.72)	91.01 (88.40-93.61)	96.14 (94.39-97.89)	95.27 (93.34-97.20)
MCC	99.47 (99.19-99.75)	99.54 (99.27-99.80)	99.17 (98.83-99.52)	88.77 (85.90-91.64)	92.17 (89.73-94.61)	93.38 (91.12-95.64)
G-Mean	99.65 (99.43-99.87)	99.75 (99.56-99.94)	99.71 (99.51-99.92)	93.02 (90.71-95.34)	96.09 (94.33-97.85)	97.75 (96.40-99.10)

Table 2. Detailed information about the proposed Auto-Keras model (trimmed table)

Layer number	Layer (type)	Output Shape	Param #	Connected to	Config
1	Input_1 (Inputlayer)	(None, 30, 35, 3)	0		
2	conv2d_1 (Conv2D)	(None, 30, 35, 64)	1792	input_1[0][0]	activation: linear, filters: 64, kernel_size: (3,3), strides: (1,1)
3	batch_normalization_1 (BatchNor)	(None, 30, 35, 64)	256	conv2d_1[0][0]	momentum: 0.99, epsilon: 0.001
4	activation_26 (Activation)	(None, 30, 35, 64)	0	batch_normalization_1[0][0]	activation: relu
5	batch_normalization_2 (BatchNor)	(None, 30, 35, 64)	256	activation_26[0][0]	momentum: 0.99, epsilon: 0.001
6	activation_1 (Activation)	(None, 30, 35, 64)	0	batch_normalization_2[0][0]	activation: relu
7	conv2d_2 (Conv2D)	(None, 30, 35, 64)	36928	activation_1[0][0]	activation: linear, filters: 64, kernel_size: (3,3), strides: (1,1)
8	batch_normalization_3 (BatchNor)	(None, 30, 35, 64)	256	conv2d_2[0][0]	momentum: 0.99, epsilon: 0.001
9	activation_2 (Activation)	(None, 30, 35, 64)	0	batch_normalization_3[0][0]	activation: relu
10	activation_3 (Activation)	(None, 30, 35, 64)	0	activation_1[0][0]	activation: relu
11	conv2d_3 (Conv2D)	(None, 30, 35, 64)	36928	activation_2[0][0]	activation: linear, filters: 64, kernel_size: (3,3), strides: (1,1)
12	conv2d_4 (Conv2D)	(None, 30, 35, 64)	4160	activation_3[0][0]	activation: linear, filters: 64, kernel_size: (1,1), strides: (1,1)
.
.
73	batch_normalization_16 (BatchNo)	(None, 30, 35, 512)	2048	add_7[0][0]	momentum: 0.99, epsilon: 0.001
74	activation_22 (Activation)	(None, 30, 35, 512)	0	batch_normalization_16[0][0]	activation: relu
75	conv2d_23 (Conv2D)	(None, 30, 35, 512)	2359808	activation_22[0][0]	activation: linear, filters: 512, kernel_size: (3,3), strides: (1,1)
76	batch_normalization_17 (BatchNo)	(None, 30, 35, 512)	2048	conv2d_23[0][0]	momentum: 0.99, epsilon: 0.001
77	activation_23 (Activation)	(None, 30, 35, 512)	0	batch_normalization_17[0][0]	activation: relu
78	activation_24 (Activation)	(None, 30, 35, 512)	0	activation_22[0][0]	activation: relu
79	conv2d_24 (Conv2D)	(None, 30, 35, 512)	2359808	activation_23[0][0]	activation: linear, filters: 512, kernel_size: (3,3), strides: (1,1)
80	conv2d_25 (Conv2D)	(None, 30, 35, 512)	262656	activation_24[0][0]	activation: linear, filters: 512, kernel_size: (1,1), strides: (1,1)
81	add_8 (Add)	(None, 30, 35, 512)	0	conv2d_24[0][0] conv2d_25[0][0]	
82	global_average_pooling2d_1 (Glo)	(None, 512)	0	add_8[0][0]	
83	dense_1 (Dense)	(None, 3)	1539	global_average_pooling2d_1[0][0]	activation: linear, units: 3

DISCUSSION

Neuroimaging plays a vital role in the diagnosis, treatment, and follow-up of brain tumors. An imaging method that can provide the necessary information in a patient with a suspected brain tumor is MRI among the radiological imaging techniques. MRI is performed to show the lesion or to rule out the presence of the lesion in the patient with suspected signs and symptoms. When assessing the precise location and localization of a tumor in a patient using MR imaging, essential information such as the type of tumor, the tumor's individual characteristics, and its effects on normal brain tissue is collected for treatment and prognosis. Similarly, it gives crucial information in tumor follow-ups such as reactive changes of a recurrent tumor and repetitive tumor separation (30).

The main basis for MR imaging of brain tumors is the mass effect and signal changes. In many brain tumors, T1 and T2 relaxation times are prolonged, and therefore the tumors are observed to be hyperintense compared to normal brain tissue in T2 images and hypointense in T1 images. MRI for brain tumor diagnosis should include at least a rapid dual-echo sequence and T1-weighted imaging before and after the application of the paramagnetic agent (30, 33).

MRI is a diagnostic method that displays the organs and structures of the body in a very safe way with high resolution without radiation. While the most essential disadvantage of this method is to cause the malfunction of the devices with magnetic effects towards the patients carrying devices such as pacemakers and infusion pumps, it has the advantage that it does not contain radiation, can be applied in children, pregnant women, cancer patients and can be repeated more than once in one patient (34). Despite its limited disadvantage, the information provided in diagnosis and follow-up by high-resolution examination of the human body causes a significant increase in the number of MRI shots today, leading to delays or misvaluations in the examination of MRI.

The goal of this study is to create a web-based program that can identify brain tumors (glioma, meningioma, pituitary adenomas) using a convolutional neural network of deep learning algorithms based on T1-weighted contrast-enhanced magnetic resonance images. It is believed that medical professionals and other health care professionals can classify brain tumors faster and more accurately, thanks to the free web-based software developed. For this, the program can be used in the detection and classification of brain tumor (i.e., glioma, meningioma, pituitary adenomas) as a clinical decision support tool. Based on the experimental results, all the calculated performance metrics are higher than 98% for the classification of brain tumor types on the training data set. Similarly, all the evaluation metrics are higher than 91% except for sensitivity and MCC for

a meningioma on the testing dataset. The proposed model is effectively capable of classifying brain tumor while considering the measured output metrics from the CNN model on the training and testing stages.

A recent research used public data sets to create a CNN-based deep learning method for the classification of brain tumors, with 233 and 73 patients on T1-weighted contrast-enhanced magnetic resonance images totaling 3064 and 516 images, respectively. The system developed in the study performs significantly with the best total accuracy rates of 96.13 percent and 98.7 percent respectively for the two datasets, and can successfully classify multi-classification tasks for a brain tumor (31). In another article, a new deep learning algorithm was built on the CNN deep learning algorithm to classify brain tumors into grade I, grade II, grade III, and grade IV. This algorithm consists of three stages: tumor segmentation, data increase, and the extraction/classification of in-depth features. Experimental results in the studied paper indicate that when applied to the augmented and original datasets, the proposed algorithm has a better performance than the present methods (32). In the previous studies, machine learning and deep learning algorithms were reported to perform well in classifying and predicting T1-weighted contrast-enhanced magnetic resonance images of brain tumors. However, the selection and development of these algorithms require a lot of time and experience when considering the machine learning/data mining applications of the recorded studies over the last years. Thus, in recent years, automatic machine learning and various modelling systems have been commonly developed (24). Authors focused on creating a content-based image retrieval method for the retrieval of brain tumors in T1-weighted contrast-enhanced MR images in another study utilizing the same brain tumor image datasets used in this study (20). Extensive studies of the described research were carried out on a broad dataset of 3604 images of three types of brain tumors, including meningiomas, gliomas, and pituitary tumors, and the mean average precision (MAP) was as high as 94.68%. In the relevant study, while the only MAP was used, the generally recommended other evaluation metrics (accuracy, sensitivity, specificity, MCC, F score, etc.) for supplementary assessment (17) in the classification of brain tumors were not reported (20). Another study using the same image sets in the current research focused on classifying three types of brain tumors in T1-weighted contrast-enhanced MR images (i.e., meningioma, glioma, and pituitary tumor), and compared three methods of classification (support vector machine (SVM), k nearest neighbors (k-NN), sparse representation-based classification (SRC)) (19). The accuracy of

the proposed model in this study outperformed SVM representing the best performance (19).

The number of MRI examinations in Organisation for Economic Co-operation and Development (OECD) countries in 2010 was the lowest (3.6 per million people) among all OECD countries in New Zealand, compared to 59.6 per million people in Turkey. In the United States, 97.6 per million people were monitored at the highest rate among all OECD countries. In 2013, in New Zealand, which had the lowest rate among OECD countries in the past three years, this rate increased to 4.3 per million people and rose to 106.9 per million people in the United States, and in Turkey, it was the highest rate (119.2 per million people) among all OECD countries (35).

Turkey ranked first among all OECD countries with a rate of 157 viewings per 1.000 people, according to the Health Statistics Yearbook 2016 of Turkey's Health Ministry. Besides, in other imaging methods interpreted by radiology experts in inpatient treatment institutions in Turkey, this rate was 188 views per 1000 people in computed tomography, 62.3 per 1000 people in ultrasonography, and 30.3 per 1000 people in doppler ultrasonography. In Turkey, on the other hand, there are just 5 radiology specialists per 100,000 people. Furthermore, international standards indicate that if a patient is not allocated for at least 15 minutes in the examination of radiology, serious problems may arise in the correct diagnosis of the patient (36).

Demanding excessive workload in a short time for radiological evaluations brings physical, spiritual, and mental burnout (37). More than half of physicians in the USA stated that they experienced one or more signs of burnout (38). One or more symptoms of burnout syndrome were observed in 79% of academic radiologists, and excessive workload and work-personal life imbalance were identified as the two factors causing the most stress (39). Also, the burnout of doctors causes a severe cost in the countries. The secondary cost for burnout in the USA was reported to be approximate \$ 4.6 billion (40).

A similar workload and burnout table to radiologists can be seen in neurosurgery specialists,

another speciality that interprets brain MRI. According to the Global Neurosurgical Workforce Map 2016 data on the website of the World Federation of Neurosurgical Societies (WFNS), while Japan had the highest rate in the world with 5.89 neurosurgeons per 100000 people, the reported rates were 1.6 per 100000 for the USA, 1.5 per 100000 for Germany, 1.26 per 100000 for Turkey, and 0.34 per 100000 for England, respectively. This rate was 0.44 per 100000 in Egypt, which has a third of the neurosurgeons available across the entire African continent, 0.061 per 100000 people in South Africa, 0.049 per 100000 in Kenya, 0.025 per 100000 in Ethiopia and 0.015 per 100000 in Tanzania, while South Sudan, Liberia, and Sierra Leone still have no neurosurgeons (41).

The necessary information about the tumor can be obtained with a brain MRI interpreted correctly by experts. However, the number of radiologists and neurosurgery specialists is not sufficient. In contrast, the number of views made every year has almost doubled every decade, with a rapid increase in the last two decades (42). Also, advanced computer-aided systems based on artificial intelligence can be used in the diagnostic and decision-making process for radiological imaging made at times outside of active working hours. Thus, burnout between radiologists can be reduced by interpreting the image in 3-4 seconds (43).

There are several limitations to our research. Our study included only T1-weighted brain MR images. Other sequences, such as contrast enhanced T1-weighted brain MRI images, would be excluded, lowering precision, sensitivity, and accuracy. Moreover this study not including histopathological confirmation. However, the experimental results obtained from the proposed system are quite successful based on the performance metrics.

In brief, the current research introduces a new public web-based program for classifying brain tumor types based on T1-weighted MR image scans by CNN deep learning algorithm. Figure 4-a and Figure 4-b respectively show the T1-weighted contrast-enhanced MR image of the Glioma tumor and the estimation results of the developed web-based software for this image.

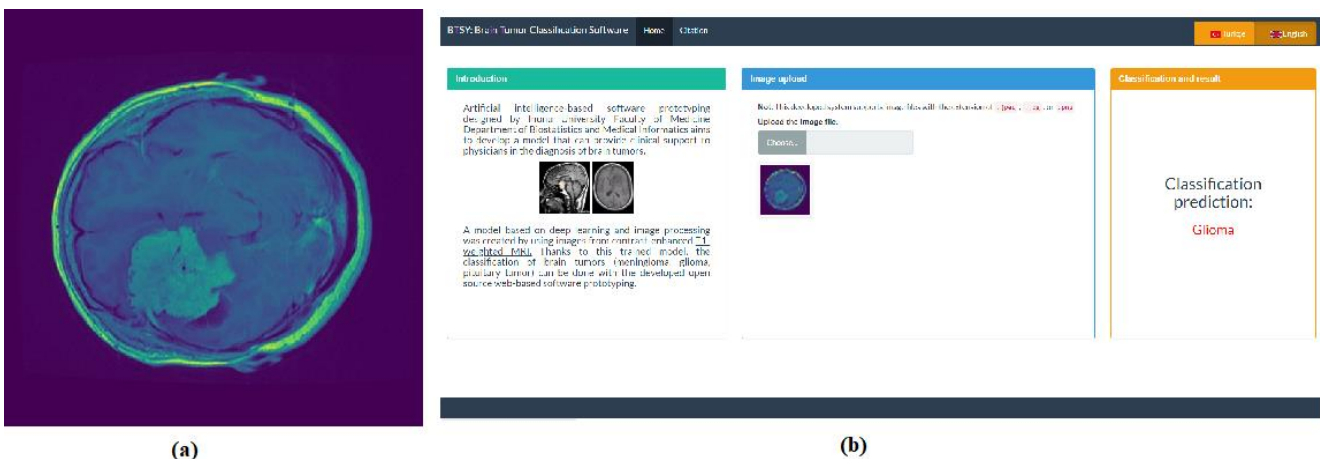


Figure 4. (a) T1-weighted contrast-enhanced MR image of the Glioma tumor, (b) The estimation results of the developed web-based software for Glioma

In the following steps, in addition to medical images of the brain tumors of patients studied in this study, it is envisaged to build a program that

can identify data sets that include brain images of healthy individuals.

REFERENCES

- Louis DN, Perry A, Reifenberger G, Von Deimling A, Figarella-Branger D, Cavenee WK, et al. The 2016 World Health Organization classification of tumors of the central nervous system: a summary. *Acta neuropathologica*. 2016;131(6):803-20.
- Wrensch M, Minn Y, Chew T, Bondy M, Berger MS. Epidemiology of primary brain tumors: current concepts and review of the literature. *Neuro-oncology*. 2002;4(4):278-99.
- Hassanipour S, Namvar G, Fathalipour M, Ghorbani M, Abdzadeh E, Zafarshampour S. The incidence of brain tumours in Iran: A systematic review and meta-analysis. *Advances in Human Biology*. 2019;9(1).
- Ostrom QT, Gittleman H, Fulop J, Liu M, Blanda R, Kromer C, et al. CBTRUS statistical report: primary brain and central nervous system tumors diagnosed in the United States in 2008-2012. *Neuro-oncology*. 2015;17(suppl_4):iv1-iv62.
- Crocetti E, Trama A, Stiller C, Caldarella A, Soffiatti R, Jaal J, et al. Epidemiology of glial and non-glial brain tumours in Europe. *European journal of cancer*. 2012;48(10):1532-42.
- Howlader N, Noone A, Krapcho M, Garshell J, Miller D, Altekruse S, et al. SEER cancer statistics review, 1975-2012. Bethesda, MD: National Cancer Institute. 2015;2015.
- Ohgaki H, Kleihues P. Population-based studies on incidence, survival rates, and genetic alterations in astrocytic and oligodendroglial gliomas. *Journal of Neuropathology & Experimental Neurology*. 2005;64(6):479-89.
- Ostrom QT, Gittleman H, Liao P, Vecchione-Koval T, Wolinsky Y, Kruchko C, et al. CBTRUS statistical report: primary brain and other central nervous system tumors diagnosed in the United States in 2010-2014. *Neuro-oncology*. 2017;19(suppl_5):v1-v88.
- Bauchet L, Ostrom QT. Epidemiology and molecular epidemiology. *Neurosurgery Clinics*. 2019;30(1):1-16.
- Mohammadzadeh A, Mohammadzadeh V, Kooraki S, Sotoudeh H, Kadivar S, Shakiba M, et al. Pretreatment evaluation of glioma. *Neuroimaging Clinics*. 2016;26(4):567-80.
- Ostrom QT, Gittleman H, Xu J, Kromer C, Wolinsky Y, Kruchko C, et al. CBTRUS statistical report: primary brain and other central nervous system tumors diagnosed in the United States in 2009-2013. *Neuro-oncology*. 2016;18(suppl_5):v1-v75.
- Jordan JT, Plotkin SR. Benign intracranial tumors. *Neurologic clinics*. 2018;36(3):501-16.
- Ezzat S, Asa SL, Couldwell WT, Barr CE, Dodge WE, Vance ML, et al. The prevalence of pituitary adenomas: a systematic review. *Cancer: Interdisciplinary International Journal of the American Cancer Society*. 2004;101(3):613-9.
- Aflorci ED, Korbonits M. Epidemiology and etiopathogenesis of pituitary adenomas. *Journal of neuro-oncology*. 2014;117(3):379-94.
- Drange MR, Fram NR, Herman-Bonert V, Melmed S. Pituitary tumor registry: a novel clinical resource. *The Journal of Clinical Endocrinology & Metabolism*. 2000;85(1):168-74.
- Harmon SA, Tuncer S, Sanford T, Choyke PL, Türkbey B. Artificial intelligence at the intersection of pathology and radiology in prostate cancer. *Diagnostic and Interventional Radiology*. 2019;25(3):183.
- Koçak B, Durmaz EŞ, Ateş E, Kılıçkesmez Ö. Radiomics with artificial intelligence: a practical guide for beginners. *Diagnostic and Interventional Radiology*. 2019;25(6):485.
- Cheng J. Brain tumor dataset. figshare Dataset. https://figshare.com/articles/dataset/brain_tumor_dataset/1512427. 2017.
- Cheng J, Huang W, Cao S, Yang R, Yang W, Yun Z, et al. Enhanced performance of brain tumor classification via tumor region augmentation and partition. *PloS one*. 2015;10(10).
- Cheng J, Yang W, Huang M, Huang W, Jiang J, Zhou Y, et al. Retrieval of brain tumors by adaptive spatial pooling and fisher vector representation. *PloS one*. 2016;11(6).
- Thomas T, Vijayaraghavan AP, Emmanuel S. *Introduction to Machine Learning. Machine Learning Approaches in Cyber Security Analytics*: Springer; 2020. p. 17-36.
- Nielsen MA. *Neural networks and deep learning*: Determination press San Francisco, CA, USA.; 2015.
- Russakovsky O, Deng J, Su H, Krause J, Satheesh S, Ma S, et al. Imagenet large scale visual recognition challenge. *International journal of computer vision*. 2015;115(3):211-52.
- Hutter F, Kotthoff L, Vanschoren J. *Automated Machine Learning*: Springer; 2019.
- Bengio Y. Gradient-based optimization of hyperparameters. *Neural computation*. 2000;12(8):1889-900.
- Bergstra J, Bengio Y. Random search for hyper-parameter optimization. *Journal of machine learning research*. 2012;13(Feb):281-305.
- Jin H, Song Q, Hu X, editors. Auto-keras: An efficient neural architecture search system. *Proceedings of the 25th ACM SIGKDD International Conference on Knowledge Discovery & Data Mining*; 2019.

28. Collette A, Tocknell J, Caswell TA, Dale D, Pedersen UK, Jelenak A, et al. H5Py/H5Py: 2.2. 0 Software <https://doi.org/10.5281/zenodo.400660>. 2017.
29. ZARARSIZ G, Akyildiz HY, GÖKSÜLÜK D, Korkmaz S, ÖZTÜRK A. Statistical learning approaches in diagnosing patients with nontraumatic acute abdomen. *Turkish Journal of Electrical Engineering & Computer Sciences*. 2016;24(5):3685-97.
30. Sartor K. MR imaging of the brain: tumors. *European Radiology*. 1999;9(6):1047-54.
31. Sultan HH, Salem NM, Al-Atabany W. Multi-Classification of Brain Tumor Images Using Deep Neural Network. *IEEE Access*. 2019;7:69215-25.
32. Sajjad M, Khan S, Muhammad K, Wu W, Ullah A, Baik SW. Multi-grade brain tumor classification using deep CNN with extensive data augmentation. *Journal of computational science*. 2019;30:174-82.
33. Curnes JT. MR imaging of peripheral intracranial neoplasms: extraaxial vs intraaxial masses. *Journal of computer assisted tomography*. 1987;11(6):932-7.
34. Wood R, Bassett K, Foerster V, Spry C, Tong L. 1.5 Tesla Magnetic Resonance Imaging Scanners Compared with 3.0 Tesla Magnetic Resonance Imaging Scanners: Systematic Review of Clinical Effectiveness: Pilot Project. 2011.
35. Yiğit V. Manyetik Rezonans Görüntüleme Sağlık Teknolojisinin Yayılımı. *Türkiye Klinikleri Sağlık Bilimleri Dergisi*. 2016;1(1):38-46.
36. DERNEĞİ TR. RADYOLOJİK TETKİK YOĞUNLUĞU, TETKİK YOĞUNLUĞUNDAN KAYNAKLANAN PROBLEMLERİN ANALİZİ ve ÇÖZÜM ÖNERİLERİ 2018. Available from: <https://www.turkrad.org.tr/assets/2018/Radyolojik-Tetik-Yogunlugu-Raporu.pdf>.
37. Cohan RH, Davenport MS. Productivity, Meet Burnout. *Academic radiology*. 2018;25(12):1513-4.
38. Shanafelt TD, Hasan O, Dyrbye LN, Sinsky C, Satele D, Sloan J, et al., editors. Changes in burnout and satisfaction with work-life balance in physicians and the general US working population between 2011 and 2014. *Mayo Clinic Proceedings*; 2015: Elsevier.
39. Ganeshan D, Rosenkrantz AB, Bassett Jr RL, Williams L, Lenchik L, Yang W. Burnout in Academic Radiologists in the United States. *Academic radiology*. 2020.
40. Han S, Shanafelt TD, Sinsky CA, Awad KM, Dyrbye LN, Fiscus LC, et al. Estimating the attributable cost of physician burnout in the United States. *Annals of internal medicine*. 2019;170(11):784-90.
41. El-Ghandour NM. Neurosurgical education in Egypt and Africa. *Neurosurgical Focus*. 2020;48(3):E12.
42. Lang K, Huang H, Lee DW, Federico V, Menzin J. National trends in advanced outpatient diagnostic imaging utilization: an analysis of the medical expenditure panel survey, 2000-2009. *BMC medical imaging*. 2013;13(1):40.
43. McDonald RJ, Schwartz KM, Eckel LJ, Diehn FE, Hunt CH, Bartholmai BJ, et al. The effects of changes in utilization and technological advancements of cross-sectional imaging on radiologist workload. *Academic radiology*. 2015;22(9):1191-8.